Electron–He_2^+ scattering calculation using the R-matrix method: resonant and bound states of He_2

2017 J. Phys. B: At. Mol. Opt. Phys. 50 115203

(http://iopscience.iop.org/0953-4075/50/11/115203)

IOP Publishing Journal of Physics B: Atomic, Molecular and Optical Physics
J. Phys. B: At. Mol. Opt. Phys. **50** (2017) 115203 (9pp) https://doi.org/10.1088/1361-6455/aa6a34

Electron–He_2^+ scattering calculation using the R-matrix method: resonant and bound states of He_2

M D Epée Epée[1], O Motapon[1,2], D Darby-Lewis[3] and J Tennyson[3]

[1] Laboratoire de Physique Fondamentale, UFD Mathématiques, Informatique Appliquée et Physique Fondamentale, University of Douala, PO Box 24157, Douala, Cameroon
[2] University of Maroua, Faculty of Science, PO Box 814 Maroua, Cameroon
[3] Department of Physics and Astronomy, University College London, Gower Street London, WC1E 6BT, United Kingdom

E-mail: j.tennyson@ucl.ac.uk

Received 15 September 2016, revised 20 March 2017
Accepted for publication 30 March 2017
Published 11 May 2017

Abstract

The UK molecular R-matrix codes are used to study electron collisions with the He_2^+ molecular ion. Full configuration interaction calculations are performed to obtain the potential energy curves of the ground X $^2\Sigma_u^+$ and the first excited A $^2\Sigma_g^+$ electronic states of He_2^+. Resonances, effective quantum numbers, and resonance widths as a function of the internuclear separation are determined for the lowest singlet $^1\Sigma_g^+$, $^1\Sigma_u^+$, $^1\Pi_g$ and $^1\Pi_u$ and triplet $^3\Sigma_g^+$, $^3\Sigma_u^+$, $^3\Pi_g$, $^3\Pi_u$ and $^3\Delta_u$ states, which are relevant for the study of the reactive collision of He_2^+ with low-energy electrons. In addition, bound states are also calculated for each symmetry of He_2 at several geometries.

Supplementary material for this article is available online

Keywords: electron molecule collisions, fusion, resonance curves, helium dimer

(Some figures may appear in colour only in the online journal)

1. Introduction

The helium molecular ion, He_2^+, was the first molecule to form in the Universe (Lepp *et al* 2002); albeit its appearance is thought to have been short-lived. Since then, it is thought to have been formed in the remnant of supernovae (Lepp *et al* 1990) and in the atmospheres of cool white dwarfs (Stancil 1994). On Earth, He_2^+ can form in cool helium-containing plasmas, including fusion plasmas, and its curves can play a role in Penning ionisation of metastable helium atoms (Garrison *et al* 1973).

In most environments where He_2^+ forms, the major destruction mechanism is dissociative recombination (DR):

$$He_2^+ + e^- \rightarrow He + He^*. \quad (1)$$

This process relies on the formation of doubly-excited, metastable states of He_2, which provide the route to dissociation. DR rates for He_2^+ have been measured in storage rings (Urbain *et al* 2005). Storage rings have also been used to study inelastic collisions between electrons and He_2^+ ions (Buhr *et al* 2008).

There have been a number of theoretical studies of electron collisions with He_2^+. These include the DR studies of Carata *et al* (1999), Royal and Orel (2005) and Royal and Orel (2007), who used He_2 curves and lifetimes computed using the Kohn variational method. These calculations are discussed further below. R-matrix calculations have also been used to study the He_2^* system. McLaughlin *et al* (1993) computed bound and continuum curves, but only of $^3\Sigma_u^+$ total symmetry. Recently, Celiberto *et al* (2016) used an R-matrix calculation to compute cross-sections for the electron-impact dissociation of He_2^+.

He_2^+ and He_2 are, respectively, three and four electron systems; they should therefore be amenable to highly accurate electronic structure calculations. In this work, we aim to compute a comprehensive and accurate set of bound and

Table 1. Comparison of energies (in Hartree) for the ground state X $^2\Sigma_u^+$ and the first excited state A $^2\Sigma_g^+$ of the He_2^+ molecular ion at the selected bond length.

State	R(*a.u*)	This work	Cencek *et al*[a]	Tung *et al*[b]	Gadea and Paidarova[c]	McLaughlin *et al*[d]	
						Truncated CI	Full CI
$X^2\Sigma_u^+$	2.0	−4.988 475 2	−4.994 402 35		−4.990 317	−4.982 802 5	−4.990 725 8
	2.042	−4.988 673	−4.994 644 2	−4.994 643	−4.990 579		
	2.5	−4.974 214 6	−4.980 371 96		−4.976 980	−4.968 760 5	−4.976 836 1
	3.0	−4.949 241 1	−4.955 776 65		−4.952 694	−4.943 661 9	−4.951 917 3
$A^2\Sigma_g^+$	2.0	−4.603 143 0			−4.605 518	−4.594 455 0	−4.604 711 1
	2.042	−4.622 843 4					
	2.5	−4.765 283 4			−4.767 643	−4.757 254 5	−4.766 982 9
	3.0	−4.835 105 2			−4.837 597	−4.827 267 8	−4.836 745 1

[a] Extrapolated value of Cencek and Rychlewski (1995).
[b] Explicitly correlated Gaussian calculation of Tung *et al* (2012).
[c] FCI calculation of Gadea and Paidarova (1996).
[d] R-matrix calculation of McLaughlin *et al* (1993), which used a (4s, 2p, 2d) Slater type orbital basis.

continuum curves for excited states of the helium dimer. These curves will form the input for future studies of key processes involving electron collisions of He_2^+, such as DR.

2. Calculations

2.1. Method

In this work, we use the R-matrix method (Tennyson 2010) as implemented in the UKRMol codes (Carr *et al* 2012). This method is based on dividing the configuration space into two distinct spatial regions (Burke 2011) by a sphere, of radius $12a_0$, centred at the centre-of-mass of the molecule. This encloses the wave function of the 3-electron target He_2^+ ion. In the inner region, the wave functions for the target plus scattering electron system ($He_2^+ + e^-$) is given by:

$$\Psi_k^{N+1}(x_1,\ldots,x_{N+1}) = \mathcal{A}\sum_{ij} a_{ijk}\,\phi_i^N(x_1,\ldots,x_N)\,u_{ij}(x_{N+1}) + \sum_i b_{ik}\,\chi_i^{N+1}(x_1,\ldots,x_{N+1}), \quad (2)$$

where $\mathcal{A}$ is the anti-symmetrization operator, u_{ij} are known as continuum orbitals, x_i is the spatial and spin coordinates of electron i, ϕ_i^N is the wave functions of the ith target state and χ_i are two-centre L^2 functions constructed as products of target occupied and virtual molecular orbitals. The variational coefficients a_{ijk} and b_{ik} are determined by diagonalizing the Hamiltonian matrix.

2.2. Target calculations

It is known that the basis sets play an important role in the quality of the calculation. We use for the present work, the cc-pVTZ Gaussian basis set for He_2^+, which includes polarisation functions. An initial set of molecular orbitals was obtained by performing self-consistent field calculations for the X $^2\Sigma_u^+$ state of He_2^+, although in practice the choice of orbitals is not important in a full configuration interaction (FCI) calculation. The two lowest He_2^+ states, X $^2\Sigma_u^+$ and A $^2\Sigma_g^+$, were included in the close-coupling expansion of the trial wave function of the scattering system; the other target states are too high in energy to contribute significantly at the collision energies considered here. Each target state was represented by an FCI wave function. Our FCI calculations performed at selected bond lengths around the equilibrium position for the ground state X $^2\Sigma_u^+$ and the first excited state A $^2\Sigma_g^+$ of the He_2^+ molecular ion (see table 1) were in very close agreement with the high-accuracy calculations of McLaughlin *et al* (1993), Cencek and Rychlewski (1995), Gadea and Paidarova (1996) and Tung *et al* (2012).

2.3. Scattering calculations

Scattering calculations used a two-term close-coupling expansion based on the FCI representation of the He_2^+ X $^2\Sigma_u^+$ and A $^2\Sigma_g^+$ target states. Continuum functions considered partial waves up to $l = 4$ (g functions) and were taken from Faure *et al* (2002). The FCI L^2 functions were generated by allowing all four electrons to occupy any target orbital subject only to the constraints of total symmetry.

Calculations were performed for singlet and triple spin symmetries and using C_{2v} point group symmetry. The below results have been recast using standard linear molecule symmetry notation. Calculations were repeated at 25 geometries in the range $R = 1.8$–6.0 a_0.

2.4. Resonance detection and fitting

For the resonant states, the R-matrix is propagated (Morgan 1984) to the distance for the results to stabilise, and then matched with a Gailitis expansion (Noble and Nesbet 1984). Here, a distance of 200.1 a_0 was used. Resonances were detected and fitted to a Breit–Wigner profile to obtain their energy (E) and width (Γ) using the programme RESON (Tennyson and Noble 1984). The calculations used an initial energy grid of 0.73×10^{-3} Ryd; upon detection of a

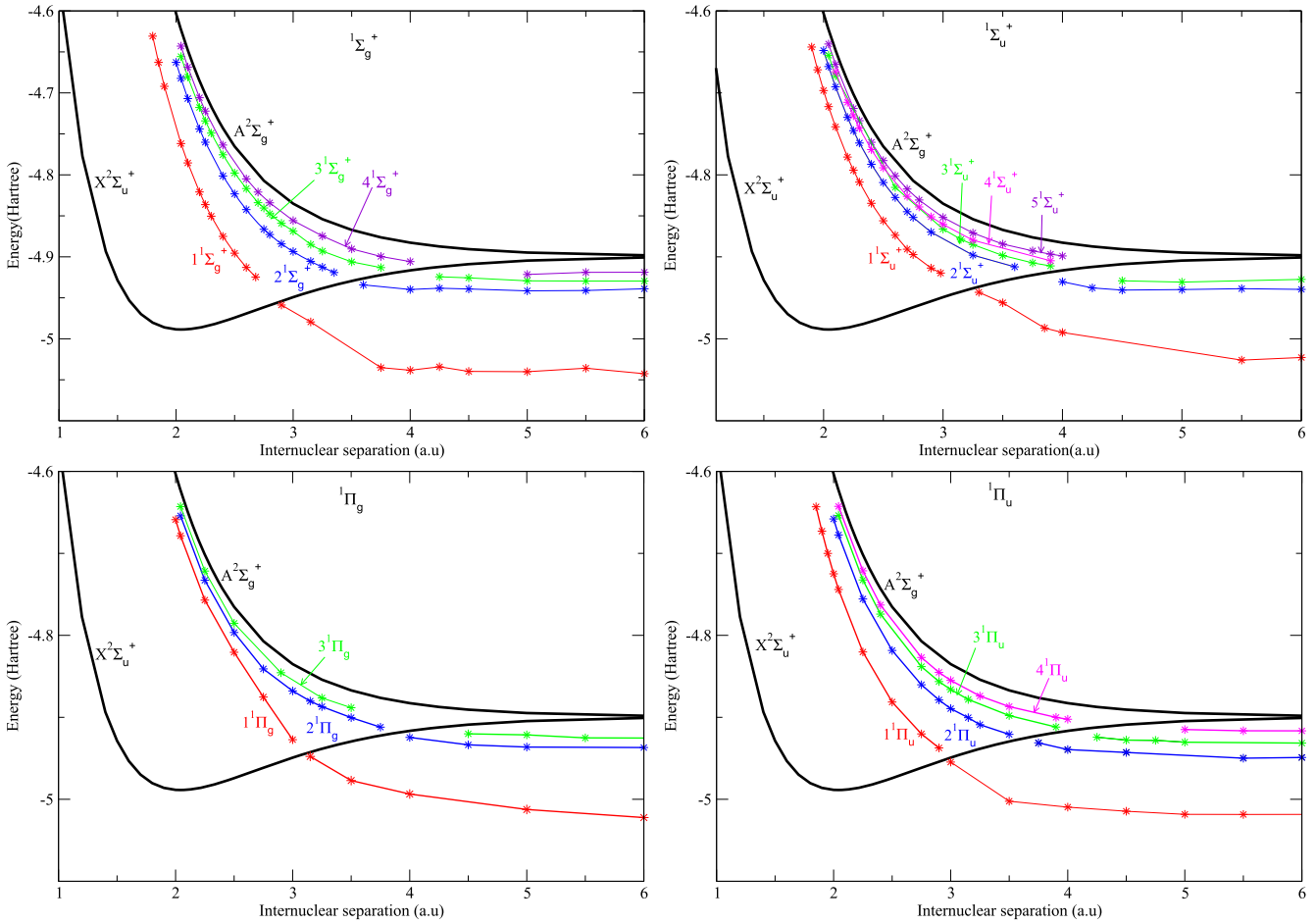

Figure 1. Electronic energy curves of He_2 resonance states of singlet symmetry, with calculated points indicated by stars. The symmetry of each set of resonances is indicated in the panel; colour is used to match the molecular state corresponding to each curve with the resonance widths given in figure 4. The two black, thick, full curves are the ground X $^2\Sigma_u^+$ and the first excited A $^2\Sigma_g^+$ states of He_2^+.

resonance, RESON then lays down an appropriate grid based on the estimated resonance width. Complex quantum defects were obtained from the resonances using the relations

$$E_r = E_t - \frac{1}{\nu^2}, \qquad \Gamma = \frac{4\beta}{\nu^3} \tag{3}$$

where E_t is the energy of the threshold to which the resonance state is associated. The effective quantum number ν is related to the real part of the quantum defect by $\nu = n - \alpha$, where n is an integer. For resonances, the complex quantum defect μ is given by $\mu = \alpha + i\beta$, where estimates of α and β, which are assumed to vary smoothly and usually with n, can be obtained by performing scattering calculations above the threshold (Seaton 1983, Tennyson 1988).

The recent study of Little and Tennyson (2014) on resonance states of N_2 found it necessary to develop an enhanced method based on time-delays to characterise N_2^* resonances (Little *et al* 2016). Here, however, the resonances are generally well spaced and the absence of extra, nearby excited target states means that it is not necessary to consider intruder states. As a result, the single, isolated resonance model assumed in the Breit–Wigner fits gives good results.

2.5. Bound states

After solving the inner region problem, the solutions were used to built the R-matrix on the boundary. Outer region wave functions were then integrated to a distance of 30.1 a_0 from where an asymptotic expansion due to Gailitis (Noble and Nesbet 1984) is used. For this work, an improved Runge–Kutta–Nystrom integration procedure, as implemented by Zhang *et al* (2011) was used. Bound states were then found using the searching algorithm of Rabadán and Tennyson (1996) with the improved nonlinear, quantum defect-based grid of Sarpal *et al* (1991).

3. Results and discussion

We present here our calculations of resonances and bound states of He_2, effective quantum numbers, and widths of singlet and triplet symmetries. Results are shown graphically, but a complete set of data is provided in a spreadsheet as supplementary material to this article. These results are compared with the quasidiabatic potentials of Royal and Orel (2005).

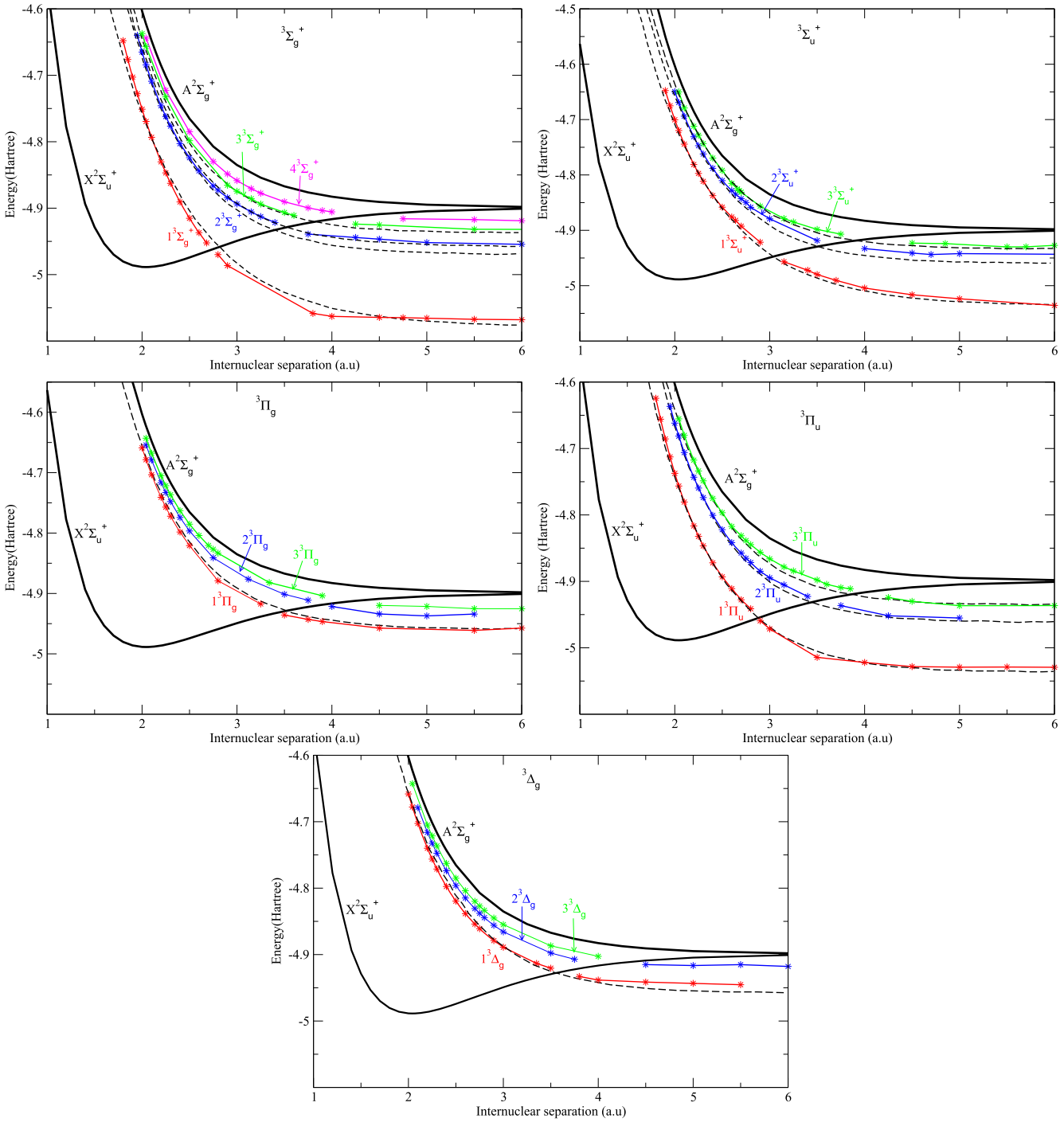

Figure 2. Electronic energy curves of He_2 resonance states of triplet symmetry with calculated points indicated by stars. The symmetry of each set of resonances is indicated in the panel; colour is used to match the molecular state corresponding to each curve with the resonance widths given in figure 6. The two black, thick, full curves are the ground X $^2\Sigma_u^+$ and the first excited A $^2\Sigma_g^+$ states of He_2^+. Dashed curves are the quasidiabatic potentials of Royal and Orel (2005).

The resonance curves of singlet total symmetries $^1\Sigma_g^+$, $^1\Sigma_u^+$, $^1\Pi_g$ and $^1\Pi_u$ are shown in figure 1. Those corresponding to triplet total symmetries $^3\Sigma_g^+$, $^3\Sigma_u^+$, $^3\Pi_g$, $^3\Pi_u$ and $^3\Delta_g$ are represented in figure 2, where they are compared with those of Royal and Orel (2005). These resonance curves are Rydberg states of the first excited state A $^2\Sigma_g^+$ of He_2^+, which correspond in the diabatic picture to neutral dissociative states of He_2. Below the crossing point between the resonances and the ion ground-state potential electronic curve, they are extended using the programme BOUND. These curves are shown in figures 1 and 2 with the same colour convention as the corresponding resonances. It is to be noted that there are an infinite number of bound Rydberg states, which converge on the He_2^+ X $^2\Sigma_u^+$ ground-state ion curve. This means that dissociating resonances undergo a series of interactions close to the crossing zone. These can be

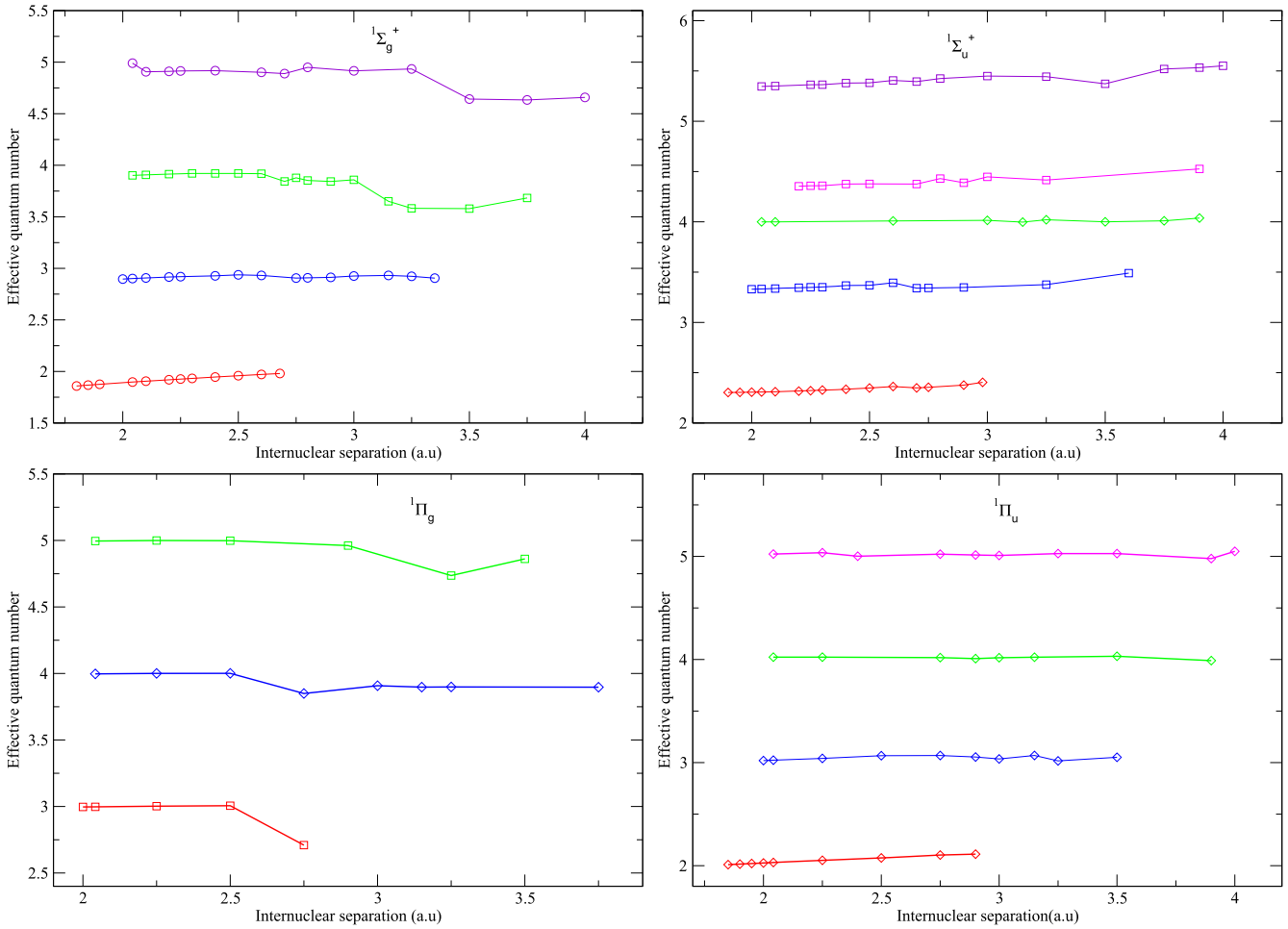

Figure 3. Effective quantum numbers corresponding to the resonances shown in figure 1 as a function of the internuclear distance R, for the $^1\Sigma_g^+$, $^1\Sigma_u^+$, $^1\Pi_g$ and $^1\Pi_u$ symmetries. The nature of the states is indicated with the symbols ∘ : s-state, ♢ : p-state, □ : d-state.

seen in the adiabatic potential energy curves of He_2 calculated by Cohen (1976). The states calculated in this zone are highly perturbed. This accounts for the lack of smoothness observed in some of our curves. In any case, the smoothness of the potential curves after the crossing point has little influence on the DR cross-section.

Figure 2 shows that there is some similarity, but not complete agreement between our curves and those of Royal and Orel (2005). However, the complex Kohn variational calculations of Royal and Orel were only performed at three internuclear distances: $R = 2.0$, 2.5 and 2.7 a_0; full curves were obtained by use of smooth functions, which matched with the appropriate asymptote. This means that direct comparison of the results of these two calculations is difficult. There are slight differences that can be accounted for by the difference in approach and choice of model. Figure 2 also shows that the crossing points of our resonances and those of Royal and Orel (2005) with the X $^2\Sigma_u^+$ ground state of the He_2^+ molecular ion are not at the same position. Our lowest $^3\Sigma_g^+$ and $^3\Pi_g$ resonance curves in figure 2 cross the ion curve at a lower energy than the corresponding one of Royal and Orel (2005). Since it is well known that the magnitude of the DR cross-sections is very sensitive to the crossing point between the dissociative state and the ion curve, for both the direct or the indirect mechanism, the shift between our curves and those of Royal and Orel (2005) should result in differences in the DR cross-section in terms of both magnitude and structure.

Effective quantum numbers and resonance widths corresponding to the resonances given in figure 1 are presented in figures 3 and 4, respectively. In the same way, effective quantum numbers and resonance widths that correspond to the resonances given in figure 2 are shown in figures 5 and 6, where they are compared with the results of Royal and Orel (2005). The approximate s, p, d, f character of the quantum defect shown in figures 3 and 5 are labelled according to the separated atom limit of the resonance state to which they belong. Our widths presented in figures 4 and 6 show significant structure. This structure is a result of the avoided crossings between the curves of the same symmetry and the interaction of many molecular states in the crossing zone, as mentioned above. The significant amount of structure in the widths could be an artefact of the Breit–Wigner fitting process used. However, our fitting programme, RESON (Tennyson and Noble 1984), computes a goodness factor, which is defined as the sum of the absolute residues for the 25 points used in the eigenphase fit. This allows a ready assessment of the quality of the fit. For the lowest two

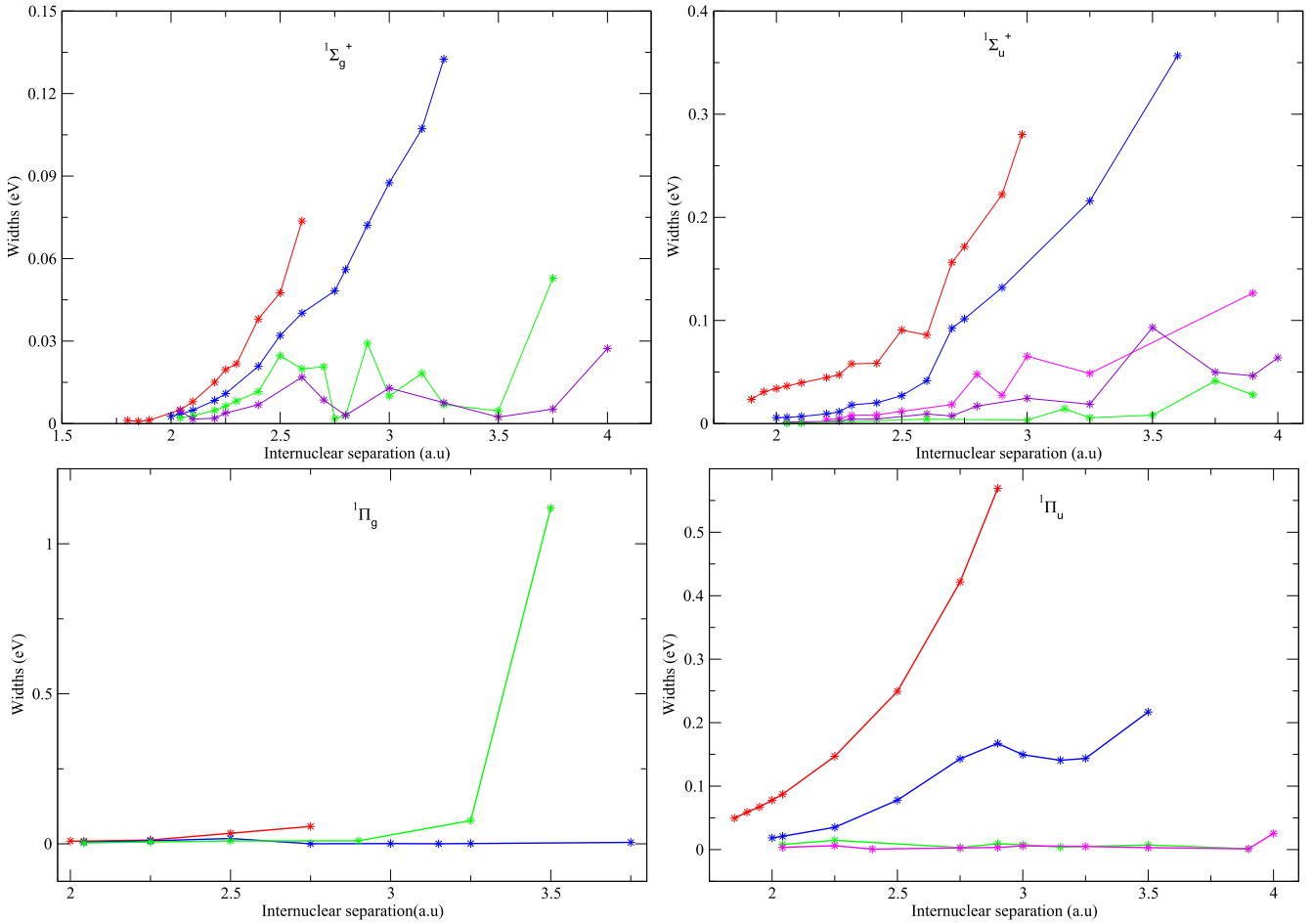

Figure 4. Resonance widths corresponding to the resonances shown in figure 1 as a function of the internuclear distance R, for the $^1\Sigma_g^+$, $^1\Sigma_u^+$, $^1\Pi_g$ and $^1\Pi_u$ symmetries.

resonances of each symmetry, the goodness factor for our fits is excellent, typically 10^{-7} rad, when the eigenphases change by π rad over the range of the fit. For some of the higher resonances this goodness factor increases; in the worst case it is 0.05 radians in which case the widths may not be well-determined. This means, however, that the structure detected in the widths of the lower-lying resonances is a genuine feature of our calculations, which can be attributed to the interaction and crossing of the resonance state as the Rydberg series converging on each threshold. These interactions are clearly visible in plots of the effective quantum numbers, figures 3 and 5. Such interactions can cause the widths to change dramatically as a function of internuclear separation. This behaviour was also found in detailed R-matrix studies performed by Little and Tennyson (2013) and Chakrabarti and Tennyson (2015) on electron collision with N_2^+ and BeH^+, respectively.

The comparison of our triplet resonance widths as a function of internuclear separation, R, with those of Royal and Orel (2005) given in figure 6 is interesting. Royal and Orel, who do not present detailed results for their singlet calculations, assumed that the widths have a Gaussian dependence on internuclear separation. Only in one case, the second resonance of $^3\Pi_u$ symmetry is this behaviour even approximately followed by our calculated results. A previous study on electron-impact vibration excitation and dissociation of N_2 (Laporta *et al* 2014) has already shown that the use of idealised, Gaussian widths can lead to significant differences compared to calculations based on the use of the true $\Gamma(R)$. The difference in the crossing points of the ion ground state and the resonance widths will probably lead to differences between the DR and excitation cross-sections obtained from our data, and those of Royal and Orel (2005).

Given the relatively simple electronic structure of the 4-electron He_2 system, it is worth considering the residual sources of uncertainty in the present calculation. Guidelines for uncertainty quantification in collision problems have recently been given by Chung *et al* (2016). Starting first with the target electronic structure: this has been treated using an FCI so, unusually, there are no issues with the convergence of the CI model beyond those of the choice of the original 1-electron basis set. Analysis of the results of table 1 show very good agreement between our model and calculations with more extended basis sets. In particular, our excitation energies differ by only about 0.01 eV from the most accurate predictions, which are due to Gadea and Paidarova (1996). This is the crucial parameter for the scattering calculation, since the resonances are associated with Rydberg series

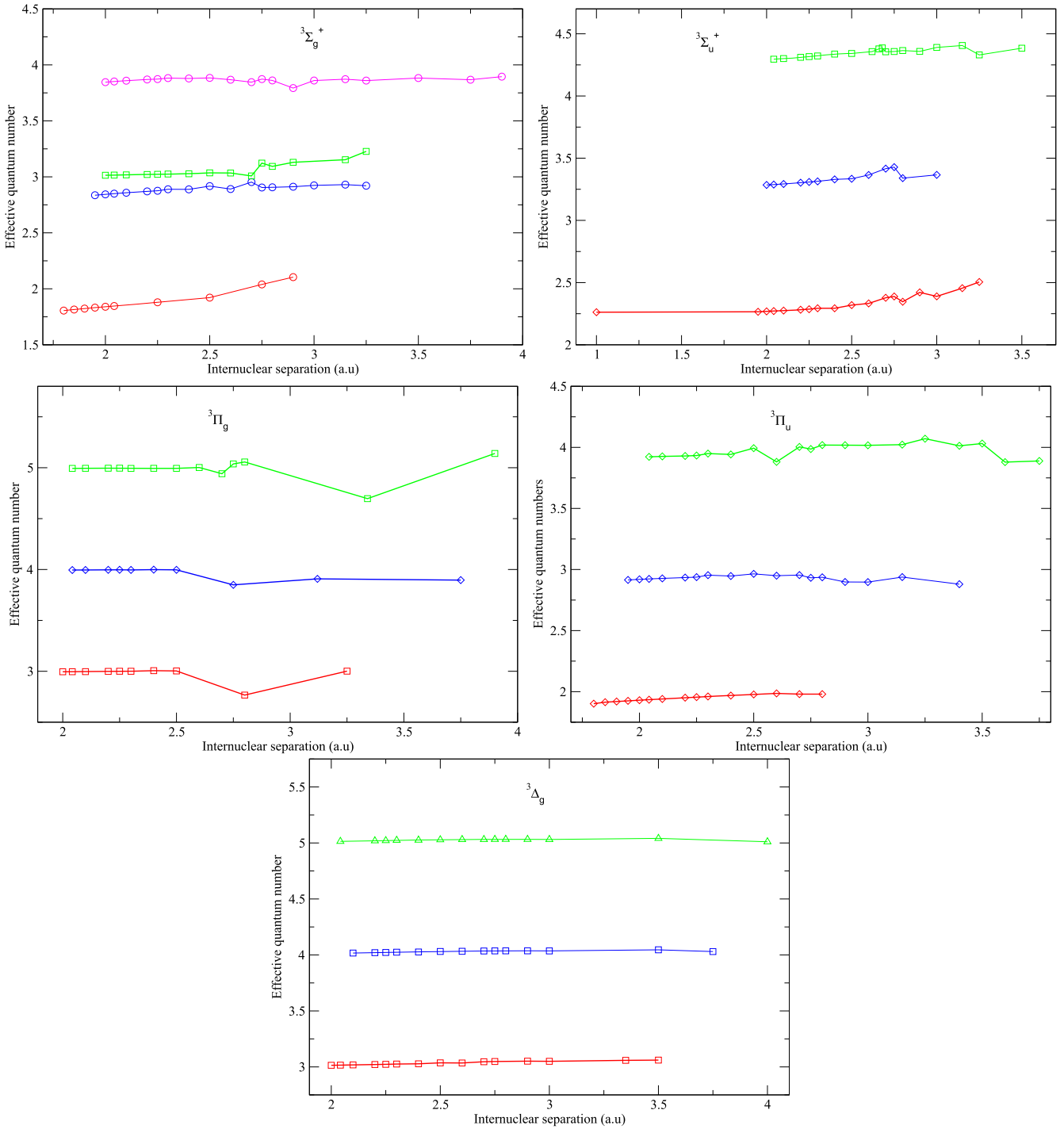

Figure 5. Effective quantum numbers corresponding to the resonances shown in figure 2 as a function of internuclear distance R, for the $^3\Sigma_g^+$, $^3\Sigma_u^+$, $^3\Pi_g$, $^3\Pi_u$ and $^3\Delta_u$ symmetries. The nature of the states is indicated with the symbols ∘ : s-state, ◊ : p-state, □ : d-state, △ : f-state.

converging on the excited A $^2\Sigma_u^+$ state. Considering the scattering calculation, again the use of an FCI model both removes issues of balance between the target and scattering calculation (Tennyson 1996) and is likely to lead to good treatment of target polarisation effects. The unusual nature of the electronic structure of He_2^+ means that there is a very large gap between the first and second electronic excited states, meaning that for low-energy calculations the truncation of the calculation at two states is unlikely to introduce any significant approximation. This is not generally true and the inclusion of higher states is usually important (Brigg *et al* 2014, Jones and Tennyson 2010). The resonance parameters presented in this work involve fitting the eigenphases to a Breit–Wigner form, which in itself can be a cause of uncertainty, particularly in the case of the resonance widths. However, as discussed above, our fits for the lowest resonances proved to be very accurate and stable. Finally, our curves show some structure as a function of bond length.

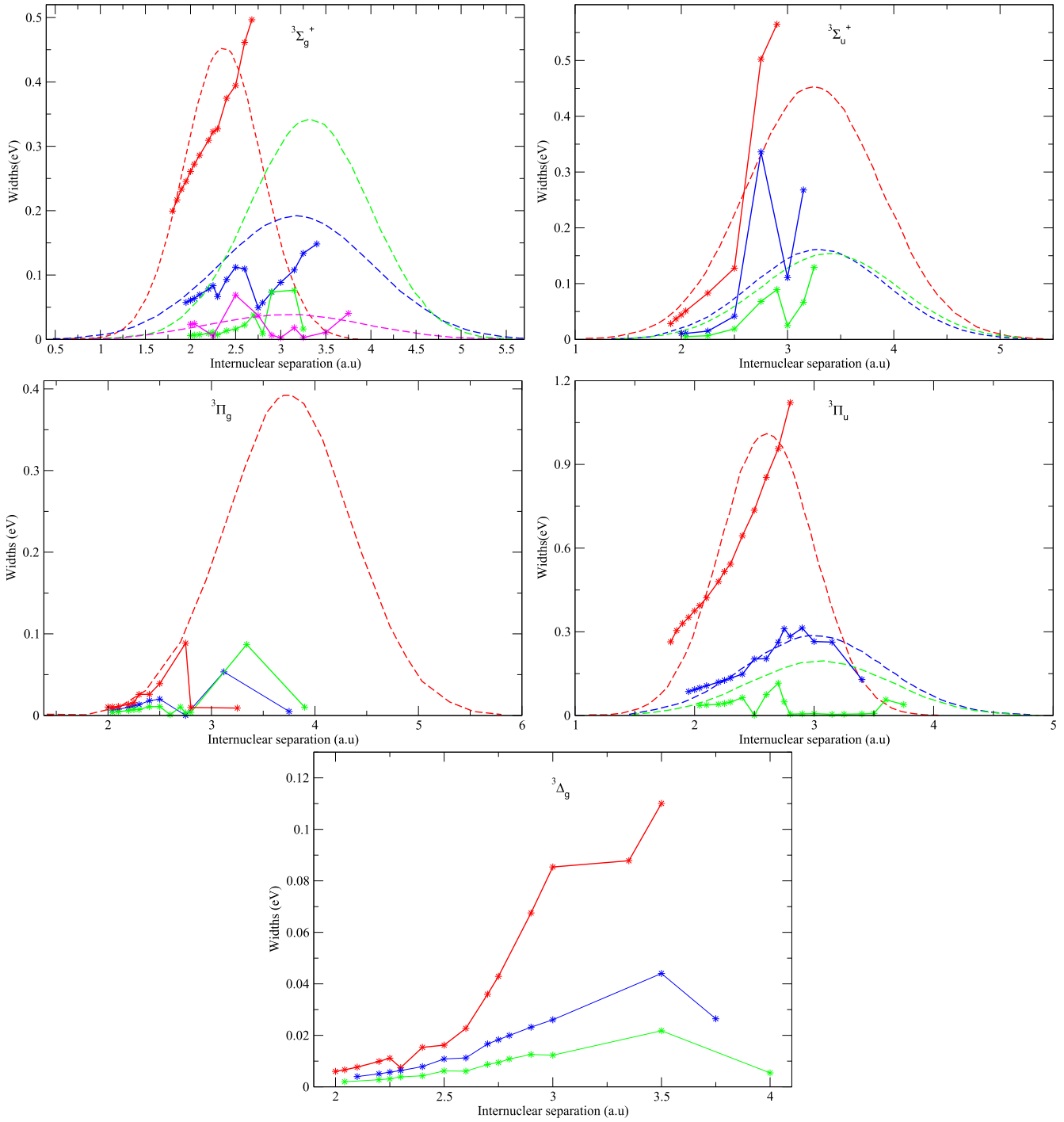

Figure 6. Resonance widths corresponding to the resonances shown in figure 2 as a function of the internuclear distance R, for the $^3\Sigma_g^+$, $^3\Sigma_u^+$, $^3\Pi_g$, $^3\Pi_u$ and $^3\Delta_u$ symmetries. Line with star: present work. Dashed curves: Royal and Orel (2005).

Such structures can be resolved by performing calculations on a very fine grid (Little and Tennyson 2014), although in practice DR calculations have thus far chosen to ignore this structure (Little *et al* 2014). All the curves presented in this paper are adiabatic and ignore any effects due to the breakdown of the Born–Oppenheimer approximation. In particular, no attempt has been made to produce so-called energy-dependent resonance widths, which result from non-adiabatic effects (Nestmann 1998). Given the reliability of other stages of the calculation, it is likely that the effect of these non-adiabatic couplings is the most significant approximation in our calculations.

4. Conclusion

Using the UK R-matrix molecular codes, we have studied electron collisions with the He_2^+ molecular ion. Electronic energy curves of resonances, widths, and effective quantum numbers were generated as a function of the geometry for the

singlet $^1\Sigma_g^+$, $^1\Sigma_u^+$, $^1\Pi_g$ and $^1\Pi_u$ and triplet $^3\Sigma_g^+$, $^3\Sigma_u^+$, $^3\Pi_g$, $^3\Pi_u$ and $^3\Delta_g$ symmetries of the He_2 molecule. Below the ion ground state, bound states were also calculated. Some differences are found between our resonance curves and widths and the former computations as well as their crossing positions. For example, at some internuclear distances, our resonance widths are larger than those of Royal and Orel (2005). Moreover, resonance curves and widths are calculated for many more bond lengths, making them suitable for appropriate use in DR computations, as the fit of the autoionization widths in this case would lead to more realistic electronic couplings. As a consequence, the use of the present data set is likely to result in differences in the cross-sections and rate coefficients predicted for some DR and related processes compared to the ones already available. The present data will be used to produce new DR and dissociative excitation cross-sections in the near future.

Acknowledgments

The authors are grateful to the International Atomic Energy Agency (IAEA, Vienna) for scientific and financial support through Contract No. 16712 with the University of Douala (CAMEROON) and via the Coordinated Research Projects 'Atomic and Molecular Data for State-Resolved Modeling of Hydrogen and Helium and their Isotopes in Fusion Plasma'. They also thank Professor Ioan F Schneider of the University of Le Havre for many helpful discussions. MDEE thanks the Department of Physics and Astronomy of the University College of London for their hospitality and a Royal Society Wolfson Research Merit Award to JT, which helped support his visit.

References

Brigg W J, Tennyson J and Plummer M 2014 *J. Phys. B: At. Mol. Opt. Phys.* **47** 185203
Buhr H *et al* 2008 *Phys. Rev.* A **77** 032719
Burke P G 2011 *R-Matrix Theory of Atomic Collisions: Application to Atomic, Molecular and Optical Processes* (Berlin: Springer)
Carata L, Orel A E and Suzor-Weiner A 1999 *Phys. Rev.* A **59** 2804–12
Carr J M, Galiatsatos P G, Gorfinkiel J D, Harvey A G, Lysaght M A, Madden D, Masin Z, Plummer M and Tennyson J 2012 *Eur. J. Phys.* D **66** 58
Celiberto R, Baluja K L, Janev R K and Laporta V 2016 *Plasma Phys. Control. Fusion* **58** 014024
Cencek W and Rychlewski J 1995 *J. Chem. Phys.* **102** 2533
Chakrabarti K and Tennyson J 2015 *J. Phys. B: At. Mol. Opt. Phys.* **48** 235202
Chung H-K, Braams B J, Bartschat K, Császár A G, Drake G W F, Kirchner T, Kokoouline V and Tennyson J 2016 *J. Phys. D: Appl. Phys.* **49** 363002
Cohen J S 1976 *Phys. Rev.* A **13** 86–98
Faure A, Gorfinkiel J D, Morgan L A and Tennyson J 2002 *Comput. Phys. Commun.* **144** 224–41
Gadea F X and Paidarova I 1996 *Chem. Phys.* **209** 281–90
Garrison B J, Miller W H and Schaefer H F 1973 *J. Chem. Phys.* **59** 3193–8
Jones M and Tennyson J 2010 *J. Phys. B: At. Mol. Opt. Phys.* **43** 045101
Laporta V, Little D A, Celiberto R and Tennyson J 2014 *Plasma Sources Sci. Technol.* **23** 065002
Lepp S, Dalgarno A and McCray A 1990 *Astrophys. J.* **358** 262–5
Lepp S, Stancil P C and Dalgarno A 2002 *J. Phys. B: At. Mol. Opt. Phys.* **35** R57–80
Little D A and Tennyson J 2013 *J. Phys. B: At. Mol. Opt. Phys.* **46** 145102
Little D A and Tennyson J 2014 *J. Phys. B: At. Mol. Opt. Phys.* **47** 105204
Little D A, Chakrabarti K, Schneider I F and Tennyson J 2014 *Phys. Rev.* A **90** 052705
Little D A, Tennyson J, Plummer M, Noble C J and Sunderland A 2016 *Comput. Phys. Commun.* **217** 137–48
McLaughlin B M, Gillan C J, Burke P G and Dahler J S 1993 *Phys. Rev.* A **47** 1967–80
Morgan L A 1984 *Comput. Phys. Commun.* **31** 419
Nestmann B M 1998 *J. Phys. B: At. Mol. Opt. Phys.* **31** 3929–48
Noble C J and Nesbet R K 1984 *Comput. Phys. Commun.* **33** 399–411
Rabadán I and Tennyson J 1996 *J. Phys. B: At. Mol. Opt. Phys.* **29** 3747
Royal J and Orel A E 2005 *Phys. Rev.* A **72** 022719
Royal J and Orel A E 2007 *Phys. Rev.* A **75** 052706
Sarpal B K, Branchett S E, Tennyson J and Morgan L A 1991 *J. Phys. B: At. Mol. Opt. Phys.* **24** 3685
Seaton M J 1983 *Rep. Prog. Phys.* **46** 167
Stancil P C 1994 *Astrophys. J.* **430** 360–70
Tennyson J 1988 *J. Phys. B: At. Mol. Opt. Phys.* **21** 805
Tennyson J 1996 *J. Phys. B: At. Mol. Opt. Phys.* **29** 6185–201
Tennyson J 2010 *Phys. Rep.* **491** 29–76
Tennyson J and Noble C J 1984 *Comput. Phys. Commun.* **33** 421–4
Tung W-C, Pavanello M and Adamowicz L 2012 *J. Chem. Phys.* **136** 104309
Urbain X, Djuric N, Safvan C P, Jensen M J, Pedersen H B, Sogaard L V and Andersen L H 2005 *J. Phys. B: At. Mol. Opt. Phys.* **38** 43–50
Zhang R, Baluja K L, Franz J and Tennyson J 2011 *J. Phys. B: At. Mol. Opt. Phys.* **44** 035203